Forward Physics-Informed Neural Networks Suitable for Multiple Operating Conditions of Catalytic CO_2 Methanation Isothermal Fixed-Bed

Son Ich Ngo* and Young-Il Lim*

**Center of Sustainable Process Engineering (CoSPE), Department of Chemical Engineering, Hankyong National University, Gyeonggi-do, Anseong-si, Jungang-ro 327, 17579 Korea (Tel: 031-670-5207; e-mail: limyi@hknu.ac.kr).*

Abstract: This study aims to develop a forward physics-informed neural network (fPINN) suitable for multiple operating conditions, representing the plug-flow reactor (PFR) model of catalytic CO_2 methanation in an isothermal fixed-bed (IFB). The fPINN was constructed by a fully connected feed-forward artificial neural network (ANN) and physical constraints including PFR governing equations, nonlinear reaction kinetics, and boundary conditions. The fPINN showed outstanding extrapolation performance for the PFR model. The speedup factor of fPINN overwhelmed the stiff ODE numerical solver when the number of spatial points became large. The fPINN can be used as a surrogate model for process optimization where multiple reactors and operating conditions are considered.

Keywords: Catalytic CO_2 methanation; Fixed-bed reactor; Reaction kinetics; Artificial neural network; Physics-informed neural network.

1. INTRODUCTION

CO_2 methanation (CM) in combination with power-to-gas (PtG) technology is an alternative to existing energy systems that could be integrated with renewable energies (Ngo and Lim, 2021, Ngo et al., 2020). CH_4 has advantages over H_2 in energy storage capacity, discharge time, safety, and transport (Schaaf et al., 2014). CM reduces carbon emissions by encouraging the synergistic integration of renewable electricity with large CO_2 footprints in industries .such as thermal power plants (Kim et al., 2021).

Among various reactor types, fixed-bed reactors (FBs) are one of the most used types for CO_2 methanation. Because the CO_2 methanation reaction is thermodynamically favored at low temperatures and high pressures (Uebbing et al., 2019), an isothermal fixed-bed reactor (IFB) without a hot spot produces high methane selectivity, exhibits stable operation, and prevents deactivation of catalyst particles through processes such as thermal degradation (i.e., nickel sintering (Rönsch et al., 2016)). However, the IFB usually requires high recycling and dilution ratios, and adiabatic reactors to maintain suitable productivity (Davis, 1981, Porubova et al., 2012). Therefore, process optimization targeting effective operating conditions such as temperature and pressure plays an important role in process design.

To develop advanced CO_2 methanation technologies, modeling and simulations have been known as effective tools for process optimization and reactor designs. The plug-flow reactor(PFR) model was widely used for representing the fixed-bed reactor (Schlereth and Hinrichsen, 2014). Fluidized-bed reactors with uniform temperature are analogous to isothermal PFR (Ngo et al., 2020, Ngo et al., 2021a, Ngo et al., 2021b).

Besides first principles and empirical elucidations, artificial neural network (ANN), data-driven models, black-box models, or surrogate models (SMs) have become an alternative approach for functional mapping between input and output data with benefits on (1) prompt predictions, (2) automated knowledge extraction, and (3) high inference accuracy (Gusmão et al., 2020, Ngo and Lim, 2021).

Recently, physics-informed neural networks (PINNs) have been reported as a suitable solver for ordinary differential equations (ODEs) and partial differential equations (PDEs) (Raissi et al., 2019). PINNs are structured by ANNs, physical laws, and automatic differentiation (AD) technique, which are constrained to respect any symmetries, invariances, or first-principle laws (Raissi et al., 2019) without domain discretization techniques and, therefore, the numerical diffusion (Warey et al., 2021). In addition, the extrapolation performance of PINNS is improved by physical constraints (Kim et al., 2020, Ngo and Lim, 2021). Nonetheless, there are few applications of PINNs in chemical process modeling, design, and optimization, which require the SM suitable for multiple operating conditions.

In this study, a forward physics-informed neural network (fPINN) coupled with AD was developed for solving a PFR model in an isothermal fixed-bed (IFB) reactor, which is suitable for multiple operating conditions and highly nonlinear reaction kinetic rates for catalytic CO_2 methanation. The results obtained from fPINN were compared with those from a common numerical solver of ODEs (ode15s in MATLAB). The extrapolation performance was analyzed by varying the range of input data for training the fPINN. It was demonstrated that the fPINN solved PFR model with multiple operating conditions and highly nonlinear chemical reaction kinetics.

2. PROCESS DESCRIPTIONS AND FORWARD PHYSICS-INFORMED NEURAL NETWORK STRUCTURE

2.1 Isothermal fixed-bed reactor for CO_2 methanation

The single-tube IFB was assumed to be processed with a coolant that was able to remove immediately the heat generated in the exothermic reaction as shown in Fig. 1. The catalytic CO_2 methanation, known as the Sabatier reaction is (Ngo and Lim, 2021)

$$CO_2 + 4H_2 \rightleftarrows CH_4 + 2H_2O, \Delta H_r^{298K} = -165 \frac{kJ}{mol} \quad (1)$$

The operating conditions were set as a temperature (T) of 350 - 450 °C, a pressure (P) of 5 bar, and a volumetric flow rate (Q) of 10 Nm^3/s. The pure gas reactants were fed to the inlet at a CO_2/H_2 molar ratio of 1/4.

2.1.1 Governing equations

The IFB was modeled as a one-dimensional (1D) plug-flow reactor at a steady-state (Ngo and Lim, 2021, Ngo et al., 2020). The momentum and energy balances were neglected because of the low-pressure drop and isothermal conditions, respectively. The mass balances for the i^{th} species ($i = CO_2$, H_2, CH_4, and H_2O) participating in the CO_2 methanation reaction in Eq. (1) are formulated as follows:

$$\frac{1}{A_t}\frac{dF_i}{dz} = \eta \nu_i r \quad (2)$$

where z (m) is the reactor tube axial position, F_i (mol/s) is the molar flow rate of a species i at position z, A_t (m^2) is the tube cross-sectional area, ν_i is the stoichiometric coefficient of species i, and r ($mol/m^3/s$) is the volumetric reaction rate. η is the effectiveness factor of the chemical reaction, which is defined as the volume-averaged reaction rate with diffusion within catalyst particles divided by the area-averaged reaction rate at the catalyst particle surface (Ngo et al., 2020). For the sake of simplicity, the value of η was assumed as one in this study.

The boundary conditions for the molar flow rate (F_i) of the species at the inlet ($z = 0$) are as follows:

$$F_i|_{z=0,\forall T \in \Omega_T} = x_{i,0} F_0 \quad (3)$$

where $x_{i,0}$ and F_0 (mol/s) are the inlet mole fraction of gas species i and the total molar flow rate of the inlet gas mixture, respectively. $\Omega_T = [350{:}2{:}450]$ °C is the range of the operating temperature, which was uniformly discretized from lower (350 °C) to higher bounds (450 °C) with an interval of 2 °C.

2.1.2 Chemical reaction kinetics

The reaction kinetics model proposed by Koschany et al. (2016) (Koschany et al., 2016) for catalytic CO_2 methanation, which was tested within a wide range of Ni contents and industrial operating conditions, was adopted in this study.

$$r = \rho_{cat}(1-\varepsilon) \frac{k \cdot p_{H_2}^{0.5} p_{CO_2}^{0.5} \left(1 - \frac{p_{CH_4} p_{H_2O}^2}{p_{CO_2} p_{H_2}^4 K_{eq}}\right)}{\left(1 + K_{OH}\frac{p_{H_2O}}{p_{H_2}^{0.5}} + K_{H_2} p_{H_2}^{0.5} + K_{mix} p_{CO_2}^{0.5}\right)^2} \quad (4)$$

$$k = 6.41 \times 10^{-5} \exp\left(\frac{93.6}{R}\left(\frac{1}{555} - \frac{1}{T}\right)\right) \quad (5)$$

$$K_{OH} = 0.62 \times 10^{-5} \exp\left(\frac{64.3}{R}\left(\frac{1}{555} - \frac{1}{T}\right)\right) \quad (6)$$

$$K_{eq} = 137 \cdot T^{-3.998} \exp\left(\frac{158.7}{RT}\right) \quad (7)$$

where R (=8.314×10^{-3} kJ/mol/K) is the gas constant, T (K) is the temperature, p_i (bar) is the partial pressure of species i, k ($mol/g_{cat}/s$) is the reaction rate constant, K_{OH} ($1/bar^{0.5}$) is the adsorption constant, and K_{eq} is the thermodynamic equilibrium constant. The catalyst density (ρ_{cat}) was set to 2300×10^3 g_{cat}/m^3_{cat}. The reaction rate in Eq. (4) including inhibition by adsorbed water (K_{ad}), equilibrium constant (K_{eq}), and non-stoichiometric reaction orders is far from the elementary reaction rate.

2.2 Forward physics-informed neural network structure

The architecture of the fPINN for the PFR model in an IFB is presented in Fig. 1. The objective of fPINN is to solve the PFR governing equations, boundary conditions, and operating pressure (P) at any given operating temperature (T).

The 50,000 collocation points were used to train the fPINN over the reactor length ($0 < z \leq 3$ m) except $z = 0$ and operating temperature ($350 \leq T \leq 450$ °C). The Dirichlet's boundary conditions were $F_{i,0} = [97.74\ 378.9\ 0\ 0]$ mol/s at the reactor inlet ($z = 0$ m and $350 \leq T \leq 450$ °C).

Since the same governing equations and training strategy with a single input PINN (Ngo and Lim, 2021) was used, the ANN structure for two inputs (z and T), four outputs (F_i) was assumed to be similar to the optimized network structure of the single input PINN composed of five hidden layers, and 256 neurons for each layer. The activation function of hyperbolic tangent (*tanh*) was applied for each hidden layer. The weights ($w_{j,k}$) and biases ($b_{j,k}$) for the j^{th} hidden layer and the k^{th} neuron are adjusted to minimize the loss function (*Loss*). The AD for spatial derivatives ($\frac{dF_i}{dz}$) was calculated via the reverse accumulation mode which propagates derivatives backward from a given output (Güneş Baydin et al., 2018). The optimized weights and biases (w^* and b^*) were obtained from the following optimization problem:

$$\{w^*, b^*\} = \underset{w,b}{\operatorname{argmin}}\{Loss = MSE_g(w,b) + MSE_b(w,b)\} \quad (8)$$

$$MSE_g(w,b) = \frac{1}{N_{train}} \sum_{j=1}^{N_{train}} \sum_{i=1}^{N_{comp}} \left[\frac{1}{A_t}\left(\frac{dF_i}{dz}\right)_j - \eta \nu_i r_j\right]^2 \quad (9)$$

$$MSE_b(w,b) = \frac{1}{N_{bnd}} \sum_{k=1}^{N_{bnd}} \sum_{i=1}^{N_{comp}} \left[F_{i,k}|_{z=0} - x_{i,0} F_0\right]^2 \quad (10)$$

where MSE_g and MSE_b are the mean squared errors for the governing equation and boundary condition, respectively. N_{train}, N_{comp}, and N_{bnd} are the number of training data sets, species (or components), and boundary condition sampling

points, respectively. The loss function (*Loss*) sums MSE_g and MSE_b.

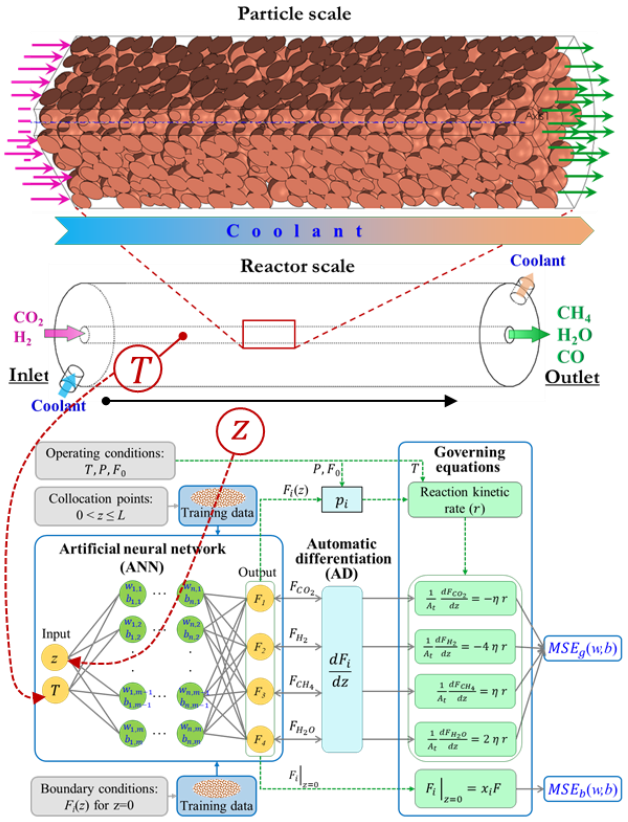

Figure 1. Plug-flow reactor (PFR) model and forward physics-informed neural network (fPINN) for CO_2 methanation (CM) in an isothermal fixed-bed (IFB) reactor.

An Adam optimizer (Kingma and Lei Ba, 2015) with an initial learning rate of 0.001 and decay rate of 0.005 was used to solve Eq. (8), which combines a stochastic gradient descent with adaptive momentum. A mini-batch size of 128, which had a minor effect on the fPINN training results, was used. The number of training epochs was set to 5,000. In the ANN, the biases (b) were initialized to zeros and the weights (w) was initialized by the commonly used heuristic called the Xavier's method (Xavier and Yoshua, 2010):

$$w_0 = U\left[-\sqrt{\frac{6}{N_{in}+N_{out}}}, \sqrt{\frac{6}{N_{in}+N_{out}}}\right] \quad (11)$$

where U is the uniform distribution in the interval of $\pm\sqrt{\frac{6}{N_{in}+N_{out}}}$. N_{in} and N_{out} are the number of neurons of the previous and present layers, respectively. The "*phylox*" pseudo-random generator with 10 rounds and a seed value of "1234" was used for reproducibility. The Sobol's quasi-random sequence generator was used for filling the collocation training points in the z space.

An ODE numerical solver (ode15s, MATLAB, The Mathworks Inc., Natick, MA, USA) with a strict relative and absolute tolerance of 1×10^{-8} was used for verifying the fPINN prediction accuracy. The accuracy of the PINN model was measured using an L_2 relative error norm between the fPINN ($F_{i,fPINN}$) and numerical ODE solver ($F_{i,ODE}$):

$$L_{2,rel} = \sqrt{\frac{\sum_{i=1}^{N_{comp}}\sum_{j=1}^{N_{test}}\left(F_{i,fPINN}^{j} - F_{i,ODE}^{j}\right)^2}{\sum_{i=1}^{N_{comp}}\sum_{j=1}^{N_{test}}\left(F_{i,ODE}^{j}\right)^2}} \quad (12)$$

where N_{test} (=1000) is the number of test data generated uniformly in the z-direction. N_{comb} (=4) is the number of specific components.

Negative intermediate outputs (F_i) appeared frequently when the stochastic gradient optimizer was used in the fPINN. In addition, the ODE system of the reactor model with chemical reaction rates was stiff. Therefore, it was desirable to avoid negative F_i and improve the convergence of the fPINN. An exponential mapping of the output values from each hidden layer (Gusmão et al., 2020) was used:

$$a_{j,l} = \exp\left(f_a\left(\sum_{k=1}^{m}\left[w_{j,k}a_{j-1,k} + b_{j,k}\right]\right)\right) \quad (13)$$

where $a_{j,l}$ is the value exiting the l^{th} neuron of the j^{th} hidden layer.

3. RESULTS AND DISCUSSIONS

Fig. 2 shows the loss function (*Loss* in Eq. 8) history over about 1 million iterations for 50,000 collocation training points. The training time was about 41 h using a single NVIDIA Quadro RTX 6000 GPU device. After 0.5 million iterations, the *Loss* converged slowly to the final value of 3×10^{-5}. The number of iterations and training points of the present study are significantly higher than the single input variable case (Ngo and Lim, 2021).

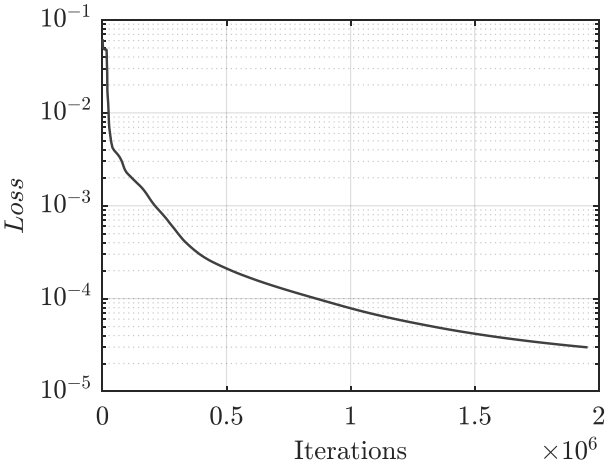

Figure 2. History of the loss function (*Loss*).

Unlike the conventional ANNs, the PINN has an extrapolation capability when applied for the range out of training data, which is similar to solving first-principle laws in a computational domain. Fig. 3 displays the performance of fPINN for interpolation and extrapolation cases. It is noted that the dashed lines are PINN predictions while the solid lines are numerical results governed by first-principle laws. Since the training data range of z and T were 0 ~ 3 m and 350 ~ 450 °C,

respectively, In Fig. 2a and 2d, the extrapolation results on both T and z are presented, while the interpolation ranges of z are marked by the shaded orange zone in the Fig. 2b and 2c. The fPINN predicted well F_i for most of ranges. However, the prediction accuracy dropped at extrapolation range and steep curves.

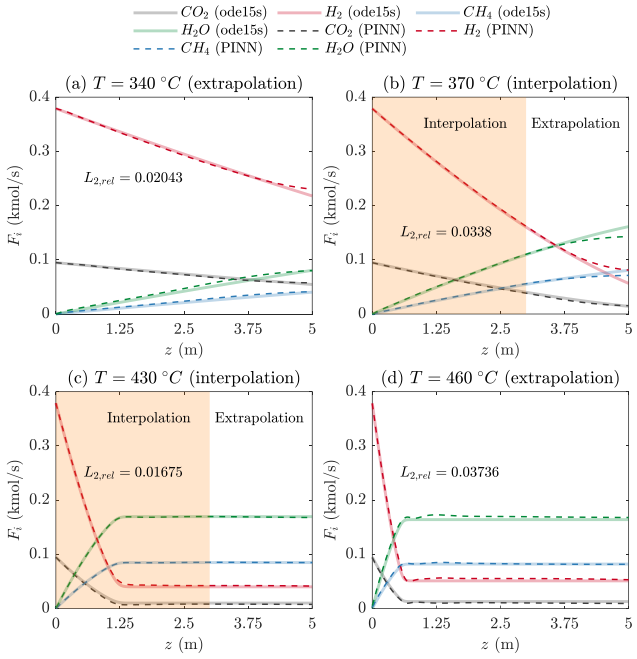

Figure 3. Performance of fPINN for two inputs and z.

Fig. 4 depicts the error map for a wide range of operating temperature (T) and reactor length (z) from 330 ºC to 470 ºC and from 0 to 5 m, respectively. The interpolation range is bounded by a red-dashed square. Since the governing equations were involved during training the network, there is no discontinuity between interpolation and extrapolation unlike common ANNs. The maximum error is about 0.3% appeared at extrapolation values of operating temperature and reactor length about 470 ºC and 0.5 m, respectively.

Even for a wide range of operating temperatures, the extrapolation capability of the fPINN is remarkable, unlike that of common ANNs (Abiodun et al., 2018). The accuracy of fPINN prediction is related to the range and distribution of training data to adapt to the complex curve behaviors (Jagtap et al., 2020). Once network parameters are optimized, the fPINN instantly predicts outputs (F_i) for any inputs (z and T), which can be used as an SM of governing equations. Differently from the discretization methods, because the training data at collocation points (z) are generated independently in the specific domain, the fPINN is suitable for solving governing equations with complex geometries or moving boundary conditions (Sun et al., 2020). Moreover, since the gradients are accurately calculated via the AD technique instead of using Taylor-series expansions, the numerical diffusion and round-off errors are minimized (Warey et al., 2021).

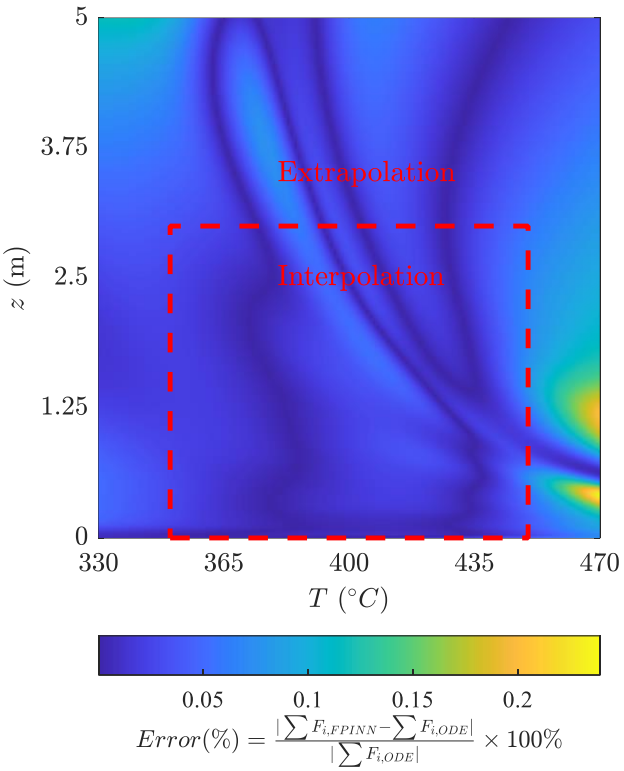

Figure 4. Error map of fPINN for a wide range of operating temperature.

Fig. 5 compares the calculation time using ODE15s and the SM obtained from the trained fPINN. The number of spatial input points was ranged from 1,000 to 50,000 with an interval of 1,000. For each number of spatial points, the SM and ODE15s were repeated for all operating temperatures from 330 to 470 ºC with an interval of 1 ºC. Such a problem is close to process optimization problems where the ODEs are solved iteratively. When the number of spatial points increased, the calculation time of the ODE numerical solver increased almost linearly. However, the calculation time of the fPINN SM is almost identical to a value lower than 0.4 s for each number of spatial points. Therefore, the speedup factor of SM obtained from fPINN became larger than the ODE numerical solver, when the number of spatial points increased.

The speedup factor and extrapolation capacity of FPINN over conventional ANNs and ODE numerical solvers are valuable in the real-time optimization problems (Francois and Bonvin, 2013, Shokry et al., 2021) and digital-twin concept (Leng et al., 2021), in which the predictions are required to be generated instantly and extrapolated widely for various operating conditions.

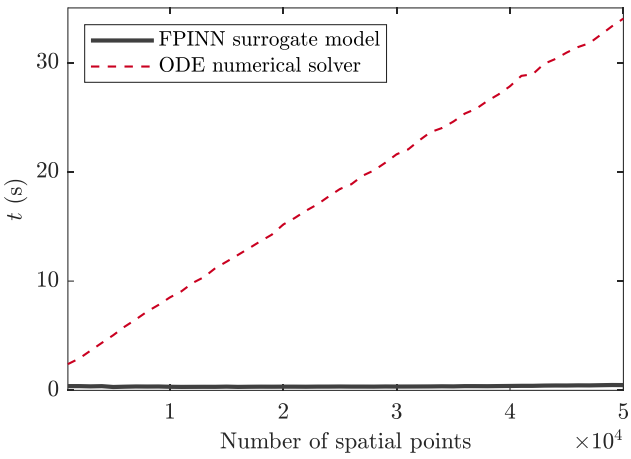

Figure 5. Comparison of calculation time between fPINN surrogate model and ODE numerical solver with respect to the number of spatial points.

4. CONCLUSIONS

A forward physics-informed neural network (fPINN) was developed for an isothermal fixed-bed (IFB) reactor model for catalytic CO_2 methanation at a wide range of operating temperatures. The fPINN was composed of a fully connected feed-forward artificial neural network (FF-ANN), automatic differentiation (AD) for derivatives, and plug-flow reactor governing equations with a stiff reaction kinetic rate. The loss function of the fPINN included two mean squared errors (MSEs) for the governing equations and boundary conditions. The one-dimensional reactor was initialized at a molar flow rate that was the same as the boundary condition at the reactor inlet. The number of iterations and training points requirements increased significantly when the operating temperature was considered as an input variable. The fPINN model exhibited an excellent extrapolation performance because the fPINN provides a solution satisfying physical laws. The speedup factor of the fPINN surrogate model over the ODE numerical solver increased when the number of spatial points increased. The current approach is useful for building a surrogate model for CO_2 methanation process design and optimization.

ACKNOWLEGEMENT

This work was supported by a National Research Foundation of Korea (NRF) grant funded by the Korean government (MEST) (Grant number: NRF-2021R1A2C1011618 and 2020R1I1A1A01074184).

REFERENCES

Abiodun, O. I., Jantan, A., Omolara, A. E., Dada, K. V., Mohamed, N. A. & Arshad, H. (2018). State-of-the-art in artificial neural network applications: A survey. *Heliyon,* 4**,** e00938.

Davis, C. R. (1981). *Methanation plant design for HTGR process heat*. United States.

Francois, G. & Bonvin, D. (2013). Chapter One - Measurement-Based Real-Time Optimization of Chemical Processes. *In:* Pushpavanam, S. (ed.) *Advances in Chemical Engineering.* Academic Press.

Güneş Baydin, A., Pearlmutter, B. A., Andreyevich Radul, A. & Mark Siskind, J. (2018). Automatic differentiation in machine learning: A survey. *Journal of Machine Learning Research,* 18**,** 1-43.

Gusmão, G. S., Retnanto, A. P., da Cunha, S. C. & Medford, A. J. (2020). Kinetics-Informed Neural Networks.

Jagtap, A. D., Kharazmi, E. & Karniadakis, G. E. (2020). Conservative physics-informed neural networks on discrete domains for conservation laws: Applications to forward and inverse problems. *Computer Methods in Applied Mechanics and Engineering,* 365**,** 113028-113028.

Kim, J., Lee, K., Lee, D., Jin, S. Y. & Park, N. (2020). DPM: A Novel Training Method for Physics-Informed Neural Networks in Extrapolation.

Kim, S., Lim, Y.-I., Lee, D., Cho, W., Seo, M. W., Lee, J. G. & Ok, Y. S. (2021). Coal power plant equipped with CO_2 capture, utilization, and storage: Implications for carbon emissions and global surface temperature. *Energy and Environmental Science,* in review.

Kingma, D. P. & Lei Ba, J. (2015). Adam: A method for stochastic optimization. *Iclr***,** 1-15.

Koschany, F., Schlereth, D. & Hinrichsen, O. (2016). On the kinetics of the methanation of carbon dioxide on coprecipitated $NiAl(O)_x$. *Applied Catalysis B: Environmental,* 181**,** 504-516.

Leng, J., Wang, D., Shen, W., Li, X., Liu, Q. & Chen, X. (2021). Digital twins-based smart manufacturing system design in Industry 4.0: A review. *Journal of Manufacturing Systems,* 60**,** 119-137.

Ngo, S. I. & Lim, Y.-I. (2021). Solution and Parameter Identification of a Fixed-Bed Reactor Model for Catalytic CO2 Methanation Using Physics-Informed Neural Networks. *Catalysts,* 11.

Ngo, S. I., Lim, Y.-I., Lee, D., Go, K. S. & Seo, M. W. (2020). Flow behaviors, reaction kinetics, and optimal design of fixed-and fluidized-beds for CO_2 methanation. *Fuel,* 275**,** 117886.

Ngo, S. I., Lim, Y.-I., Lee, D. & Seo, M. W. (2021a). Flow behavior and heat transfer in bubbling fluidized-bed with immersed heat exchange tubes for CO_2 methanation. *Powder Technology,* 380**,** 462-474.

Ngo, S. I., Lim, Y.-I., Lee, D., Seo, M. W. & Kim, S. (2021b). Experiment and numerical analysis of catalytic CO_2 methanation in bubbling fluidized bed reactor. *Energy Conversion and Management,* 233**,** 113863.

Porubova, J., Bazbauers, G. & Markova, D. (2012). Modeling of the Adiabatic and Isothermal Methanation Process. *Environmental and Climate Technologies,* 6**,** 79-84.

Raissi, M., Perdikaris, P. & Karniadakis, G. E. (2019). Physics-informed neural networks: A deep learning framework for solving forward and inverse problems involving nonlinear partial differential equations. *Journal of Computational Physics,* 378**,** 686-707.

Rönsch, S., Schneider, J., Matthischke, S., Schlüter, M., Götz, M., Lefebvre, J., Prabhakaran, P. & Bajohr, S. (2016).

Review on methanation – From fundamentals to current projects. *Fuel,* 166**,** 276-296.

Schaaf, T., Grünig, J., Schuster, M. R., Rothenfluh, T. & Orth, A. (2014). Methanation of CO2 - storage of renewable energy in a gas distribution system. *Energy, Sustainability and Society,* 4**,** 2-2.

Schlereth, D. & Hinrichsen, O. (2014). A fixed-bed reactor modeling study on the methanation of CO_2. *Chemical Engineering Research and Design,* 92**,** 702-712.

Shokry, A., Medina-González, S., Baraldi, P., Zio, E., Moulines, E. & Espuña, A. (2021). A machine learning-based methodology for multi-parametric solution of chemical processes operation optimization under uncertainty. *Chemical Engineering Journal,* 425**,** 131632.

Sun, L., Gao, H., Pan, S. & Wang, J.-X. (2020). Surrogate modeling for fluid flows based on physics-constrained deep learning without simulation data. *Computer Methods in Applied Mechanics and Engineering,* 361**,** 112732-112732.

Uebbing, J., Rihko-Struckmann, L. K. & Sundmacher, K. (2019). Exergetic assessment of CO_2 methanation processes for the chemical storage of renewable energies. *Applied Energy,* 233-234**,** 271-282.

Warey, A., Han, T. & Kaushik, S. (2021). Investigation of Numerical Diffusion in Aerodynamic Flow Simulations with Physics Informed Neural Networks. *arXiv,* 2103.03115**,** 9-9.

Xavier, G. & Yoshua, B. (2010). *Understanding the difficulty of training deep feedforward neural networks*. PMLR.